NASA/TM—2007-214990

Fracture Strength of Single-Crystal Silicon Carbide Microspecimens at Room and Elevated Temperature

Noel N. Nemeth
Glenn Research Center, Cleveland, Ohio

William N. Sharpe, Jr.
Johns Hopkins University, Baltimore, Maryland

Glenn M. Beheim and Laura J. Evans
Glenn Research Center, Cleveland, Ohio

Osama M. Jadaan
University of Wisconsin, Platteville, Wisconsin

October 2007

NASA STI Program . . . in Profile

Since its founding, NASA has been dedicated to the advancement of aeronautics and space science. The NASA Scientific and Technical Information (STI) program plays a key part in helping NASA maintain this important role.

The NASA STI Program operates under the auspices of the Agency Chief Information Officer. It collects, organizes, provides for archiving, and disseminates NASA's STI. The NASA STI program provides access to the NASA Aeronautics and Space Database and its public interface, the NASA Technical Reports Server, thus providing one of the largest collections of aeronautical and space science STI in the world. Results are published in both non-NASA channels and by NASA in the NASA STI Report Series, which includes the following report types:

- TECHNICAL PUBLICATION. Reports of completed research or a major significant phase of research that present the results of NASA programs and include extensive data or theoretical analysis. Includes compilations of significant scientific and technical data and information deemed to be of continuing reference value. NASA counterpart of peer-reviewed formal professional papers but has less stringent limitations on manuscript length and extent of graphic presentations.

- TECHNICAL MEMORANDUM. Scientific and technical findings that are preliminary or of specialized interest, e.g., quick release reports, working papers, and bibliographies that contain minimal annotation. Does not contain extensive analysis.

- CONTRACTOR REPORT. Scientific and technical findings by NASA-sponsored contractors and grantees.

- CONFERENCE PUBLICATION. Collected papers from scientific and technical conferences, symposia, seminars, or other meetings sponsored or cosponsored by NASA.

- SPECIAL PUBLICATION. Scientific, technical, or historical information from NASA programs, projects, and missions, often concerned with subjects having substantial public interest.

- TECHNICAL TRANSLATION. English-language translations of foreign scientific and technical material pertinent to NASA's mission.

Specialized services also include creating custom thesauri, building customized databases, organizing and publishing research results.

For more information about the NASA STI program, see the following:

- Access the NASA STI program home page at *http://www.sti.nasa.gov*

- E-mail your question via the Internet to *help@sti.nasa.gov*

- Fax your question to the NASA STI Help Desk at 301–621–0134

- Telephone the NASA STI Help Desk at 301–621–0390

- Write to:
  NASA Center for AeroSpace Information (CASI)
  7115 Standard Drive
  Hanover, MD 21076–1320

NASA/TM—2007-214990

Fracture Strength of Single-Crystal Silicon Carbide Microspecimens at Room and Elevated Temperature

Noel N. Nemeth
Glenn Research Center, Cleveland, Ohio

William N. Sharpe, Jr.
Johns Hopkins University, Baltimore, Maryland

Glenn M. Beheim and Laura J. Evans
Glenn Research Center, Cleveland, Ohio

Osama M. Jadaan
University of Wisconsin, Platteville, Wisconsin

National Aeronautics and
Space Administration

Glenn Research Center
Cleveland, Ohio 44135

October 2007

Acknowledgments

This work was sponsored by the Combustion Sub Task of the Subsonic Fixed Wing Project at the NASA Glenn Research Center. The authors appreciate the contributions of talented Hopkins undergraduates Angelo Santiago and Ryan McCaffrey who performed most of the tests.

This work was sponsored by the Fundamental Aeronautics Program at the NASA Glenn Research Center.

Level of Review: This material has been technically reviewed by technical management.

Available from

NASA Center for Aerospace Information
7115 Standard Drive
Hanover, MD 21076–1320

National Technical Information Service
5285 Port Royal Road
Springfield, VA 22161

Available electronically at http://gltrs.grc.nasa.gov

Fracture Strength of Single-Crystal Silicon Carbide Microspecimens at Room and Elevated Temperature

Noel N. Nemeth
National Aeronautics and Space Administration
Glenn Research Center
Cleveland, Ohio 44135

William N. Sharpe, Jr.
Johns Hopkins University
Baltimore, Maryland 21218

Glenn M. Beheim and Laura J. Evans
National Aeronautics and Space Administration
Glenn Research Center
Cleveland, Ohio 44135

Osama M. Jadaan
University of Wisconsin
Platteville, Wisconsin 53818

Abstract

Three shapes of tensile specimens were tested—curved with a very low stress concentration factor and straight with either a circular hole or an elliptical hole. The nominal thickness was 125 μm with a net section 100 μm wide; the overall length of these microspecimens was 3.1 mm. They were fabricated by an improved version of deep reactive ion etching, which produced specimens with smooth sidewalls and cross sections having a slightly trapezoidal shape that was exaggerated inside the holes.

The novel test setup used a vertical load train extending into a resistance furnace. The specimens had wedge-shaped ends which fit into ceramic grips. The fixed grip was mounted on a ceramic post, and the movable grip was connected to a load cell and actuator outside the furnace with a ceramic-encased nichrome wire. The same arrangement was used for tests at 24 and at 1000 °C.

The strengths of the curved specimens for two batches of material (made with slightly different processes) were 0.66 ± 0.12 GPa and 0.45 ± 0.20 GPa respectively at 24 °C with identical values at 1000 °C. The fracture strengths of the circular-hole and elliptical-hole specimens (computed from the stress concentration factors and measured loads at failure) were approximately 1.2 GPa with slight decreases at the higher temperature.

Fractographic examinations showed failures initiating on the surface—primarily at corners. Weibull predictions of fracture strengths for the hole specimens based on the properties of the curved specimens were reasonably effective for the circular holes, but not for the elliptical holes.

Introduction

There are many applications where the combination of microelectromechanical systems (MEMS) and high-temperature operation offer significant technological advantages. Some examples are shirt-button-sized gas turbines, postage-stamp-sized rockets, and miniature pressure sensors—all experiencing temperatures of 1000 °C or higher. The immediate barrier is the lack of materials that can withstand the temperatures and are amenable to the specialized manufacturing processes of MEMS. Candidate materials must be chemically inert and capable of maintaining strength at high temperature. Silicon carbide has the potential to meet these requirements. In an excellent review entitled “Material Issues in MEMS,”

Spearing (ref. 1) states the advantages of silicon carbide (SiC) as high temperature capability along with 'much higher stiffness, hardness, toughness, and wear resistance' when compared to other common MEMS materials.

Silicon carbide based MEMS can be fabricated by chemical vapor deposition of SiC into molds or by plasma etching of SiC films (typically polycrystalline) or wafers (poly or single crystalline). However, silicon carbide fabrication technology is less mature than the well-developed ones used for silicon or polysilicon. The immediate challenge is to develop and validate processes for manufacturing silicon carbide MEMS.

Mechanical properties need to be measured with specimens that are similar in size to MEMS components and are made by the same processes. Common ceramic products are designed to withstand compression, but MEMS materials must withstand tension to permit a wide range of designs. Further, since failures of mechanical components usually initiate at stress concentrations, the tensile specimens must include notches or holes that mimic the geometry of these devices. Fracture strength is a valid measure of the efficacy of a manufacturing process. The experimental challenge is then to develop a high-temperature test method that can measure the fracture strengths of tiny brittle specimens with stress concentrations.

The NASA Glenn Research Center is addressing these challenges. The objectives of this research are fourfold:

- Develop fabrication processes that can produce SiC specimens similar in size and shape to components that would be used in high-temperature MEMS applications,
- Develop test methods and measure the fracture strength of this brittle material using smooth specimens and specimens with stress concentrations at 24 and 1000 °C,
- Correlate fabrication processes with the fracture strength response,
- Evaluate the capability of Weibull statistics to predict the strength of this brittle material at stress concentrations.

Development of the fabrication processes began with polycrystalline SiC. It is well-suited for mechanical microstructures which will be used in harsh environments; however, more expensive single-crystal SiC must be used if high temperature SiC electronics are to be integrated with SiC microstructures. A large number of parameters are involved in the deep ion reactive etching (DRIE) of SiC, and establishing a suitable process is challenging. Five process batches were run using polycrystalline SiC, and three of them produced suitable straight, curved, and notched specimens. Those were tested at room temperature only, and the processes, test procedures, and results are published in reference 2.

In this work, single-crystal SiC micro-scale tensile test specimens with high aspect ratios were fabricated and tested at 24 and 1000 °C. The results of the first group of specimens—referred to here as Batch 6—were reported in references 3 and 4. Subsequently, an improved time-multiplexed etch passivate (TMEP) process was used to fabricate a second set of single-crystal SiC specimens—Batch 7. This paper provides detailed results from both Batch 6 and Batch 7.

Mechanical failures tend to originate at changes in shape, so specimens were designed to include stress concentrations to not only measure the change in fracture strength as the highly stressed volume gets smaller, but to study the ability to predict localized response from smooth-specimen data. The smooth specimens have a gentle curvature in the gage section to avoid failure at the grip ends and will be labeled **curve** specimens in this paper. The two other designs have circular and elliptical through-holes in the center of the gage section and will be labeled **circle** and **ellipse.** The test matrix is therefore two process batches, three specimen shapes, and two temperatures.

	Curve		Circle		Ellipse	
	24 °C	1000 °C	24 °C	1000 °C	24 °C	1000 °C
Batch 6	X	X	X	X	X	X
Batch 7	X	X	X	X	X	X

Following a brief review of previous work, the three specimen designs and the manufacturing processes are described. Dimension control is important, and the specimen dimension measurements are presented. The experimental setup and test method is unique—particularly the high-temperature aspect—and is described in some detail. Numerous tests were conducted, as is necessary for a brittle material, and these are presented simply as their means and standard deviations. A limited fractographic analysis is included to give some insight as to the fracture origins. A more sophisticated approach to data analysis and prediction using the Ceramic Analysis and Reliability Evaluation of Structures/*Life* Prediction (CARES/*Life*) approach is given in a separate section. Some concluding remarks on the implications of these results for high-temperature MEMS complete the paper.

Background

Silicon carbide has several advantages for high temperature applications (ref. 5 contains over 1000 references) and these advantages apply to certain MEMS applications (refs. 6 and 7). Its high stiffness (roughly three times that of polysilicon) makes it a good candidate for the high Q required in radio frequency (RF) microdevices. Degradation in hostile environments is greatly reduced by its chemical inertness. That property also makes it easy to fabricate microdevices on silicon substrates because the etchants used in common processing of silicon and polysilicon don't attack the silicon carbide structure. Its thermal conductivity is much higher than silicon, which can be an advantage in microelectronics. However, it is the strength of silicon carbide that is of interest here, and research in this area has been limited—particularly at high temperature. In fact, lack of high-temperature properties of both silicon and polysilicon has hampered the development of mechanical systems such as microturbines (ref. 8).

Bulk silicon carbide at room temperature has a compressive strength of 0.57 to 1.38 GPa and a tensile strength of 0.03 to 0.14 GPa (ref. 9), but tests on thin or thick films are scarce. Tensile testing is preferred for structural materials because it creates a uniform state of stress and strain and enables their direct measurement; however, the gripping and alignment issues make tensile tests difficult for brittle materials. Indirect measurements of the residual stress and Young's modulus of thin-film SiC have been made by bulge testing of diaphragms (ref. 10), bending tests (ref. 11), and resonant beam tests (ref. 12). However, none of these tests measured the strength of the thin-film material.

Jackson et al. (ref. 13) conducted tensile tests on thin (0.8 and 1.7 μm thick) films of epitaxial 3C silicon carbide. The gage sections of the specimens were 600 μm wide and 4 mm long, and they were tested in a setup that enabled measurement of axial and lateral strain by laser interferometry. Young's modulus, Poisson's ratio, and fracture strength were determined. Two different processes were used to make the specimens at Case Western Reserve University—micromolding for the 0.8 μm ones and reactive ion etching (RIE) for the 1.7 μm ones. The average fracture strengths were 1.19 ± 0.53 GPa and 1.65 ± 0.39 GPa respectively. Specimens of the same planar shape, but thicker at 20 to 40 μm, were fabricated by micromolding at Massachusetts Institute of Technology (MIT) in two batches (ref. 14). The fracture strengths were 0.49 ± 0.20 GPa and 0.81 ± 0.23 GPa. Two observations about these two studies are worth noting. First, the thinner specimens (ref. 13) tend to be stronger than the thicker ones (ref. 14). Second, the coefficient of variation (standard deviation divided by mean) is quite large, reaching almost 50% in one case. This is not surprising for such small brittle specimens.

The earlier tests on polycrystalline silicon carbide are reported in reference 2 where the manufacturing process and the test method are described in detail. Briefly, the tensile microspecimens 3.1 mm long were produced by DRIE of wafers nominally 150 μm thick. The ends of the specimens were wedge-shaped to fit into matching inserts in the aluminum grips of a miniature horizontal test machine that produced a stress versus displacement plot—not a stress-strain curve. The Weibull characteristic strengths from three process runs were 0.42, 0.53, and 0.88 GPa—showing improvements in the methods. The average fracture strengths for the last process run, which had the best sidewall features, were: straight 0.38 ± 0.13 GPa, curved 0.47 ± 0.15 GPa, notched 0.78 ± 0.28 GPa. These results show a clear increase in the strength of the material as the size of the highly stressed region decreases.

The Weibull analyses in reference 2 were performed using the CARES/*Life* program originally developed at NASA. It is a stand-alone program that requires the input of finite element analysis results in order to assess component reliability. The program calculates the various Weibull parameters and then predicts the strength of the component. Incorporating all this into a design methodology shows that one can take baseline material properties from uniaxial tensile tests and predict the overall strength of complicated components (refs. 15 to 17). This is commensurate with traditional mechanical design, but with the addition of Weibull statistics. Details and access to CARES/*Life* are available in reference 17 and standardized methods for estimating Weibull parameters can be found in ASTM C1239.

This paper extends previous research in three ways—the material is single crystal silicon carbide, an improved manufacturing process is used, and strength is measured at both 24 and 1000 °C.

Specimen Design, Material, and Manufacture

The key to tensile testing is a specimen design that enables effective gripping. Wedge-shaped specimen ends that fit into inserts in the grips is a design that was developed earlier by Sharpe et al. (ref. 18) for metal microspecimens. A traditional tensile specimen has a straight gage section, but there was concern that a brittle specimen would break at the stress concentrations where it faired into the ends. This indeed turned out to be the case roughly half the time when tests were attempted on polycrystalline straight-gage-section specimens (ref. 2). Therefore a specimen with a gentle curvature and smaller net cross section, but that still produced a uniform stress in the middle of the gage section (labeled curve) was used. A circular-hole and an elliptical-hole specimen (labeled circle and ellipse) were designed to generate localized stress concentrations.

Figure 1 is a schematic of the basic geometries used for the microtensile specimens. The flared-end is the gripping section of the specimen, and the gage section length is 1.3 mm with a net cross section of 0.1 mm by 0.125 mm. From left to right in the figure these are (a) curve, (b) circle, and (c) ellipse designs. These generate stress concentration factors, K_n, relative to the net cross section of (a) 1.01, (b) 2.3, and (c) 4.5, respectively based on results from finite element analysis. The curve specimen was 0.1 mm at its narrowest point at the center. The central circular hole was also 0.1 mm in diameter, and the central ellipse was 0.1 mm across its major axis (perpendicular to the load axis) and 0.05 mm across its minor axis for a ratio of 2:1. Both these latter designs were 0.2 mm wide so that the net cross section was the same for all three geometries. The curve specimen geometry was the baseline for predicting the response of the other two geometries.

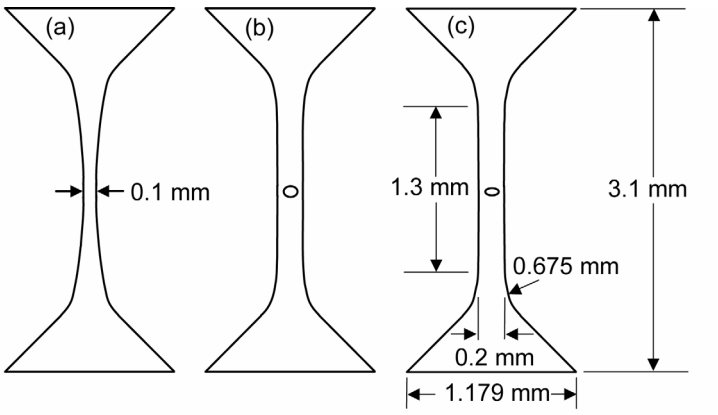

Figure 1.—Basic schematic of the microtensile specimens; (a) curve, (b) circle, (c) ellipse. The gage section is 1.3 mm in length.

The specimens were micromachined from wafers of research grade 6H polytype silicon carbide with a 3.5° off-axis orientation from Cree Materials in Durham, North Carolina (ref. 19). This is a hexagonal material, and the tensile axis was oriented parallel to the $\{10\bar{1}0\}$ flat on the wafer. The 50.8 mm diameter wafers were originally 370 μm thick, but were lapped and polished from the backside to produce the final thickness of 125 μm.

DRIE was accomplished with an inductively coupled plasma etcher (STS Multiplex Inductively Coupled Plasma (ICP)). The etch mask was electroplated nickel 10 μm thick. Wafers were etched using a TMEP process (ref. 20), a technique widely used in the DRIE of silicon in order to form structures with high aspect ratios (etch depth divided by lateral feature size) (ref. 21). This technique alternates fluorine-plasma etching of the substrate with the deposition of a passivating polymer layer to produce an anisotropic profile (i.e., vertical sidewalls). In fluorine-plasma etching of silicon, the high reactivity of silicon with fluorine radicals causes fast lateral etching. In TMEP etching of silicon, this lateral etching is inhibited by coating the sidewalls with polymer, thereby producing the desired anisotropic profile. Silicon carbide, on the other hand, is relatively inert, and appreciable etch rates in fluorine plasmas are obtained only when the SiC surface is subjected to ion bombardment. Since the ions are well collimated and strike only the horizontal surfaces of the substrate, the SiC etch process is inherently anisotropic. However, the lateral etch rate, while small, is not zero, which causes roughening of the sidewalls during long-duration etches. For this reason, and also to obtain better control over the sidewall slope, TMEP etching of SiC was attempted. Key process parameters (e.g., pressure, RF power, duration of deposition step) were adjusted in order to produce the smoothest and most nearly vertical sidewalls.

The TMEP process enabled fabrication of specimens with reduced sidewall roughness and more nearly vertical sidewalls compared to specimens that were fabricated using an etch-only DRIE process (ref. 2). SF_6 was used as the etching gas, while C_4F_8 was used to deposit a fluorocarbon polymer film, which protected the sidewalls from lateral etching. The TMEP process was used to fabricate two batches of single-crystal SiC tensile test specimens, designated Batch 6 and Batch 7. For Batch 6, pressure was held constant at approximately 12 mTorr, with 1000 W coil power and 75 W platen power applied during the etching step. The etch rate was 0.16 μm/min. Sides of the specimens were rougher than the unetched top and bottom surfaces, and exhibited vertical striations. Even so, the surfaces etched using the TMEP process showed a significant decrease in roughness compared to SiC specimens fabricated using etch only processes (ref. 2).

Figure 2 shows a circular-hole Batch 6 specimen. The sidewalls of Batch 6 specimens were not precisely vertical but sloped outwards with increasing etch depth. The outward slope was more pronounced in the etched holes because of the increased likelihood that etch products will not escape a deep hole but will instead redeposit on the wall. This is illustrated by figure 3, which shows a partially fabricated circular-hole specimen. In Batch 6, the size of the elliptical holes, in particular, was significantly reduced from the top to the bottom side of the specimen.

Subsequent to the fabrication of Batch 6, the ICP etcher was upgraded with a higher power coil generator and a series of experiments was performed to develop a new TMEP process that would provide a higher etch rate and more uniform, from top to bottom, stress concentrating holes. Batch 7 was fabricated using this modified TMEP process, in which the pressure was held at approximately 17 mTorr, with 2000 W coil power and 150 W platen power applied during the etching step. The greater coil power provided an etch rate of 0.25 μm/min. In Batch 7, the sidewalls were indeed more vertical and the dimensions of the elliptical holes were reduced less, from top to bottom. A new flaw, however, was introduced in Batch 7. At the end of the etch, when the SiC wafer was etched through to free up the

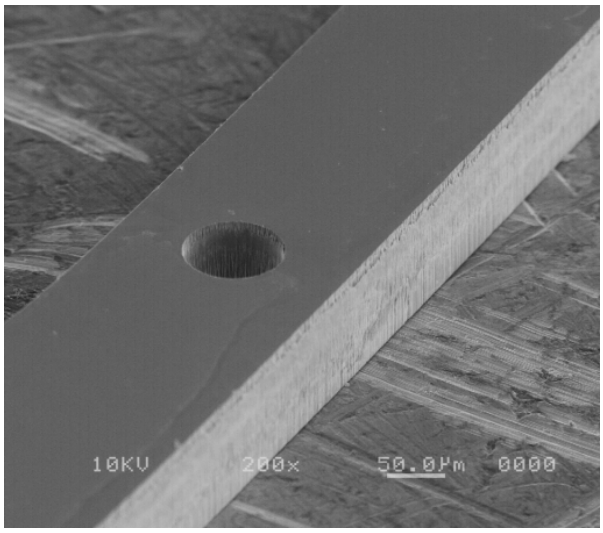

Figure 2.—Circle specimen from Batch 6.

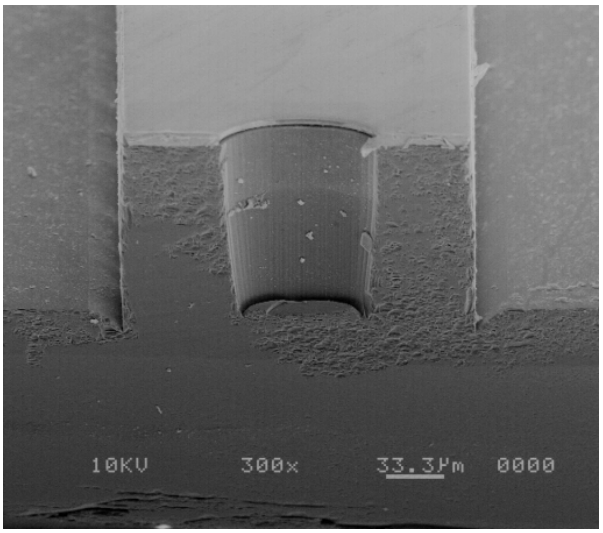

Figure 3.—Cross section of a circle specimen etched partway into a SiC wafer using the Batch 6 TMEP process.

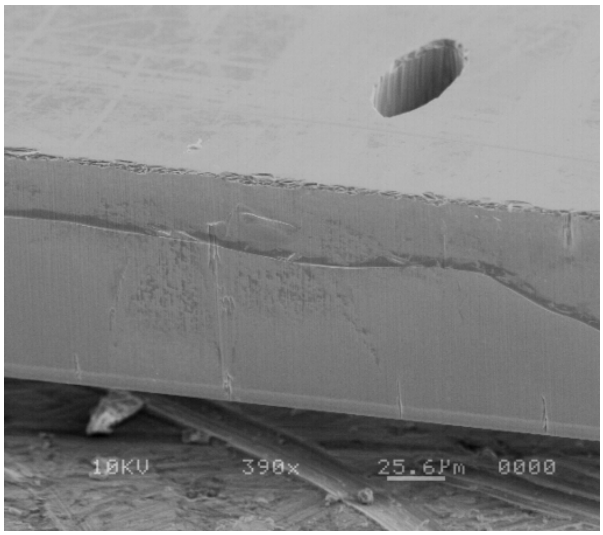

Figure 4.—Ellipse specimen of Batch 7, showing chipping at bottom edge (top side is down).

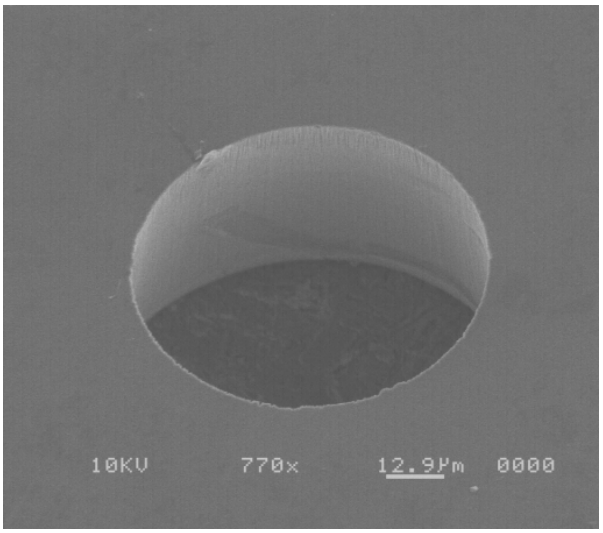

Figure 5.—Bottom side of Batch 7 circle specimen.

individual specimens, substantial over-etching was used to try to eliminate a jagged lip around the bottom edge of the specimens. This did not occur in Batch 6, possibly because the Batch 6 process produced a greater etching enhancement at the base of the sidewall (microtrenching), as is visible in figure 3. For some of the Batch 7 specimens, the several-micron-wide lip was not eliminated until the specimens were ultrasonically cleaned after removal of the nickel etch mask. This caused the lip to break off, chipping the bottom edge of the specimen as can be seen in figure 4, and to a lesser extent, figure 5.

Specimen Dimension Measurements

Any manufacturing process needs to produce the desired shape and dimensions, and part of the process development is assessing the variation in the results. Table 1 summarizes the extensive dimension measurements for both Batch 6 and 7. The adjustable reticle of a Vickers microhardness tester was used to measure the Batch 6 specimens, and an Olympus metallurgical microscope with measurement software was used for Batch 7.

TABLE 1.—RATIOS OF DIMENSIONS FROM TOP TO BOTTOM OF SPECIMENS

Batch/specimen type	Ratio of widths: top/bottom	Ratio of major axes: top/bottom	Ratio of minor axes: top/bottom
Batch 6/curve	0.894 ± 0.034	N/A	N/A
Batch 7/curve	0.881 ± 0.035	N/A	N/A
Batch 6/circle	0.939 ± 0.025	1.184 ± 0.060	N/A
Batch 7/circle	0.930 ± 0.019	1.186 ± 0.056	N/A
Batch 6/ellipse	0.934 ± 0.020	1.238 ± 0.030	1.631 ± 0.311
Batch 7/ellipse	0.927± 0.021	1.174 ± 0.054	1.364 ± 0.137

Note that bottoms of the specimens are wider than the tops, but the tops of the holes are wider than the bottoms. The Batch 7 process significantly reduced the narrowing of the elliptical hole minor axis, as shown in table 1. Despite extensive experimentation, a SiC TMEP process was not found which could produce a precisely vertical sidewall. The outward slope achieved using TMEP of SiC is distinctly different from that previously obtained using an etch-only process, in which the sidewall had a significant inward (re-entrant) slope (ref. 2).

Experimental Setup and Procedure

The wedge-shaped ends of the specimens of figure 1 are designed to fit into inserts in grips in a miniature testing machine. The gentle curvature of the curve specimens and the stress concentrations in the other two contained fracture to the center portions away from the grip ends. The original version of the room-temperature test machine had a horizontal load train with the movable grip attached to a load cell mounted on a motor-driven translation stage (ref. 2). The grips were aluminum with the movable one supported by a linear air bearing to eliminate friction.

A completely different system is required for high-temperature testing. First, the specimen must be heated and this is accomplished in a resistive furnace. Second, the grips must withstand the temperature; these were machined from Aremcolox 502-1400—a fully fired alumina maintaining its strength to 1650 °C. Third, the load train is turned vertically to eliminate friction. Figure 6 is a schematic of the setup. The furnace is custom-made from Thermcraft, Inc. with a 2 in. diameter by 4 in. long hot zone; it is closed at the top and sits on an insulated base that has a 2 in. diameter through hole. The base is mounted on an aluminum platform 12 in. above a table. A half-inch alumina post extends up into the hot zone of the furnace to serve as the frame for the load train. The upper ceramic grip is attached to the post. The lower grip is attached to a nichrome wire encased in a small ceramic tube and connected at the bottom to a load cell mounted on a piezoelectric actuator. A capacitance probe (Capacitec HPC-401-A-L2-5-B-D with 410-SC-BNC amplifier) records the vertical displacement of the actuator. This wire is mounted inside another, larger, tube with a small ceramic guide plate on top for alignment. Temperature is measured by a thermocouple through a hole in the side of the furnace and controlled by a Micromega controller from Omega Engineering, Inc.

Figure 7 shows the grip end of the specimen as it fits into the ceramic grip insert. The force from the grip is transferred to the sides of the wedges away from the transition into the straight gage section. Mounting the specimen in a vertical load train is more difficult than in a horizontal one, and figure 8 helps explain the procedure. The top grip is removed and placed horizontally so that one end of the specimen can be inserted in the insert. A ceramic plate and bolt (the lower bolt head in the figure) covers the insert to hold the specimen loosely in place. This grip is then fastened to the ceramic post with a bolt and washer shown at the top of the figure. The lower grip is then raised so that the bottom end of the specimen can be inserted into it. Finally, the specimen is pushed to the back of the inserts with a wire on the end of a micromanipulator and a very small force is applied by the actuator to hold the specimen in place. This is all a rather delicate procedure, but works well without damage to the specimen.

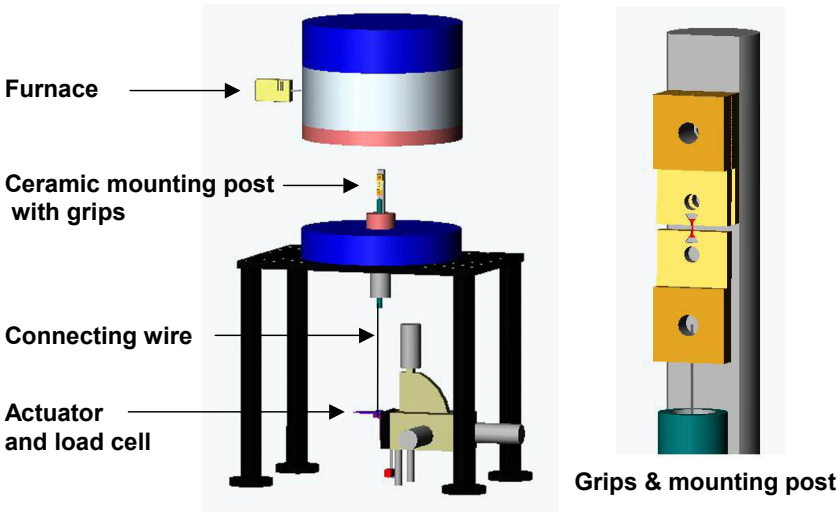

Figure 6.—Schematic of the high-temperature setup.

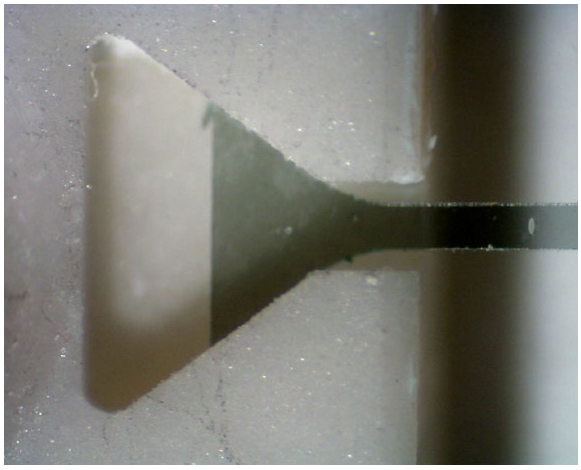

Figure 7.—Specimen end in ceramic grip insert.
The gage section is 200 μm wide.

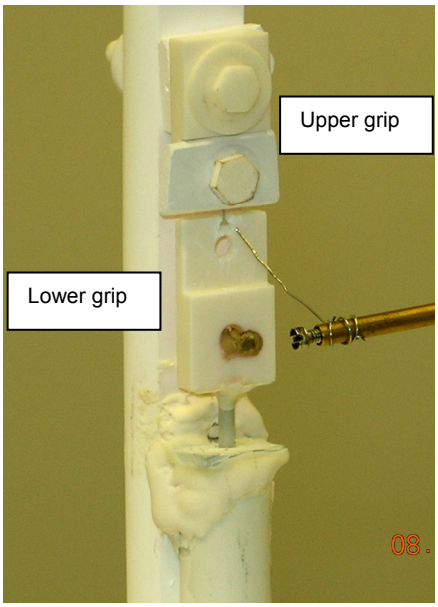

Figure 8.—Closeup of grips and specimen.
The ceramic post is 12.5 mm in diameter.

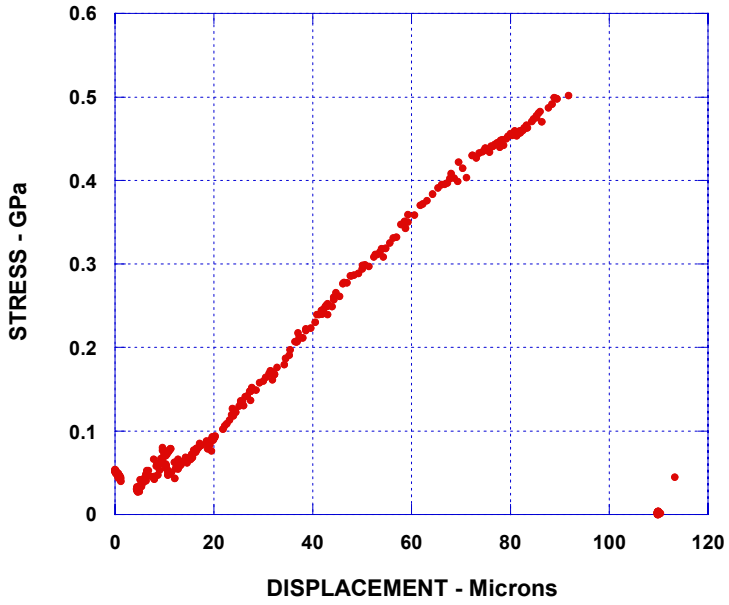

Figure 9.—Force versus actuator displacement
for a circular-hole specimen at 1000 °C.

Once the specimen is in place, a computer program in Agilent Visual Engineering Environment (VEE) controls the piezoelectric actuator to apply and record the force in the specimen and the displacement of the actuator. The resulting force-displacement curve is displayed on the computer screen. For high-temperature tests, the furnace is turned on after the specimen is in place. The connecting wire expands as it is heated, so a VEE feedback program monitors the force and adjusts the actuator to maintain the force at its initial set value. It takes about 15 minutes for the specimen to reach 1000 °C, and the temperature is held there for 10 minutes to stabilize the furnace before testing. The temperature is held

± 5 °C during the test. Figure 9 is an example of a force-displacement record for a circle specimen at 1000 °C. The displacement is almost exclusively due to the elongation of the connecting wire.

Strength Results

Investigation using finite element analysis concluded that the value of $K_n = 2.32$ for the circle configuration is essentially independent of the dimensional variations among the individual specimens and was used to compute the fracture stresses for all hole specimens. However, it was found that K_n for the ellipse specimen configuration depends significantly on the individual specimen dimensions, and thus the strength for each specimen was computed based on measured force at failure, its own trapezoidal dimensions and net stress concentration factor obtained via finite element analysis. The results are shown in tables 2 and 3 and figure 10. All fracture stresses were determined from the failure load and stress concentration factor regardless of the actual locations of fracture initiation.

TABLE 2.—FRACTURE STRENGTH RESULTS FOR BATCH 6

	Curve		Circle		Ellipse	
	24 °C	1000 °C	24 °C	1000 °C	24 °C	1000 °C
Number of tests	19	9	19	10	16	8
Average, GPa	0.662	0.656	1.241	1.180	1.229	0.945
Standard deviation, GPa	0.122	0.200	0.339	0.338	0.375	0.218
Coefficient of variation	18%	30%	27%	29%	31%	23%

TABLE 3.—FRACTURE STRENGTH RESULTS FOR BATCH 7

	Curve		Circle		Ellipse	
	24 °C	1000 °C	24 °C	1000 °C	24 °C	1000 °C
Number of tests	12	12	9	9	14	13
Average, GPa	0.453	0.448	1.230	1.052	1.480	1.051
Standard deviation, GPa	0.203	0.206	0.294	0.224	0.467	0.338
Coefficient of variation	45%	46%	24%	21%	32%	32%

The curve specimens from Batch 7 are actually weaker and show more scatter than those from Batch 6. The circle specimens show basically the same strength as well as slightly smaller scatter. The ellipse specimens of Batch 7 show higher strengths—presumably as a result of better fidelity than in Batch 6. There is no decrease in strength with temperature for the curve specimens; the values are almost exactly the same in each batch. However, there is a slight decrease in the strength at 1000 °C versus at 24 °C for the circle specimens and a larger decrease for the ellipse ones.

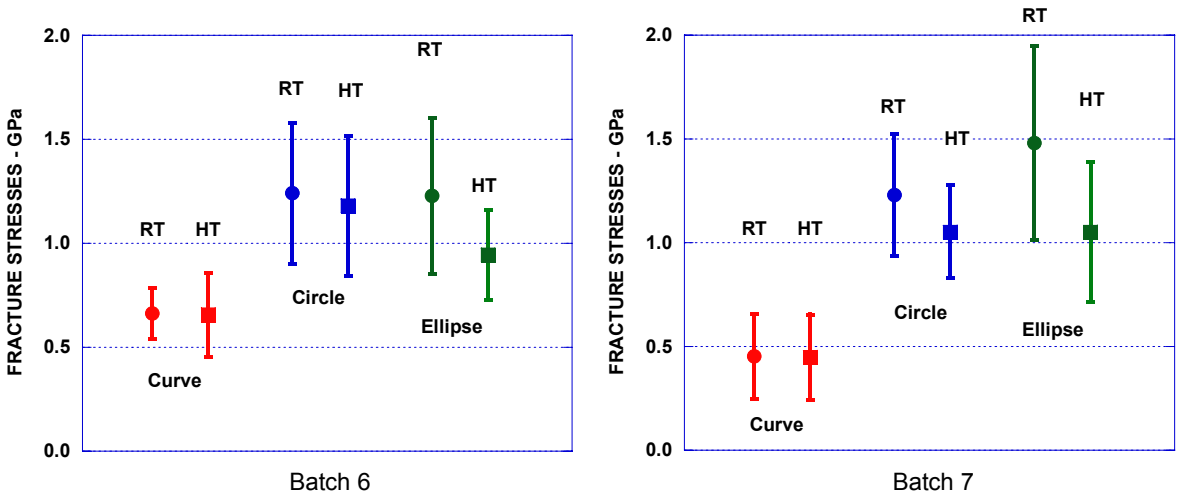

Figure 10.—Fracture strength results.

Fracture Surface Examination

A high majority of the curved specimens failed within the gage section (29/31 at 24 °C and 16/20 at 1000 °C), and similarly most of the specimens with stress concentrations failed in the hole region. The fracture surface of three specimens from each of the six combinations of Batch 7 (18 total) were examined in a Hitachi field emission scanning electron microscope (FE-SEM). All had broken in the gage section if curved and at the stress concentration of a hole or ellipse, and all fracture surfaces were perpendicular to the loading axis and were basically flat. Typical images are shown in figures 11 to 14.

Figures 11 and 12 show two curve specimens after fracture—one at each temperature. The non-rectangular shape of the cross section is readily apparent in figure 11; in fact, the fracture appears to have originated at the upper left-hand corner where the sidewall actually tapers in a little bit. The fracture surface in figure 12 is not as perfectly flat, and the fracture may have originated midway across the bottom edge. Note the deep striations along the side; these were seen in many of the specimens.

Similar to figure 11, figure 13 shows a flat surface on a circle specimen. The bottom of the specimen shows that some sections perpendicular to the flat side of the specimen broke off. This was observed in one other specimen, and it is not known whether this triggered the failure or happened afterward. Figure 14 shows an ellipse specimen tested at high temperature. There is no obvious failure origin, and the debris

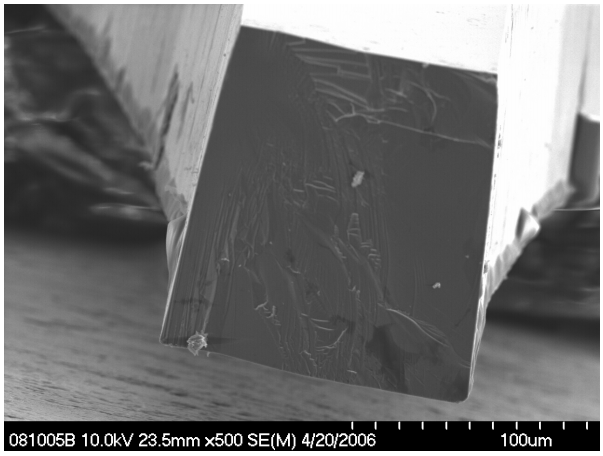

Figure 11.—24 °C curve specimen.

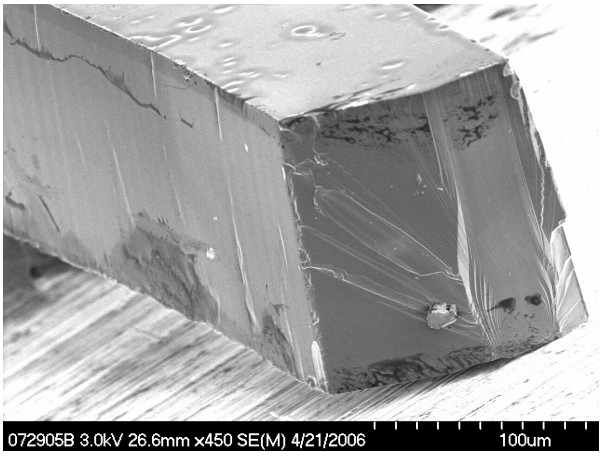

Figure 12.—1000 °C curve specimen.

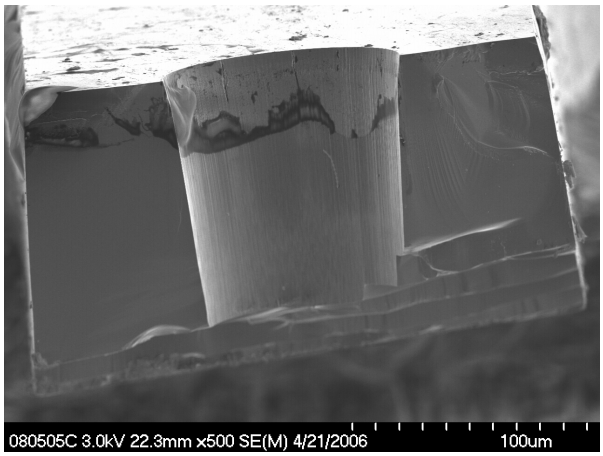

Figure 13.—24 °C circle specimen.

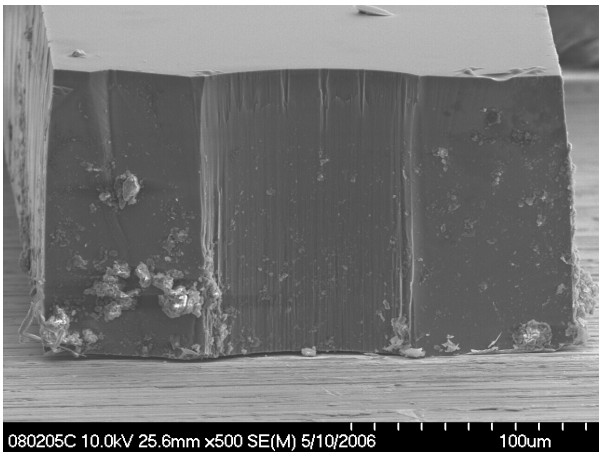

Figure 14.—1000 °C ellipse specimen.

accumulated after failure. The striations inside the ellipse are also very evident. It is important to note that examination of all the specimens showed no difference in the fracture surface morphology between those tested at room temperature and at high temperature. This observation, coupled with the strength results, demonstrates the potential for silicon carbide in high-temperature MEMS.

CARES/*Life* Analysis

The CARES/*Life* software describes the probabilistic nature of brittle material strength using the Weibull cumulative distribution function. This approach is described in two earlier papers (refs. 2 and 22) for micro-scale structures and details of the methodology are given in (refs. 16 and 17). In this report the curve specimens are used as a baseline to predict the strength response for the circle and ellipse specimens. For uniaxially stressed components the 2-parameter Weibull distribution for surface residing flaws describes the component fast-fracture failure probability, P_f, as

$$P_f = 1 - \exp\left[-\frac{1}{\sigma_0{}^m} \int_A \sigma\ (x,y)^m\ dA \right] \tag{1}$$

where A is the surface area, $\sigma(x,y)$ is the uniaxial stress at a point location on that surface, and m and σ_0 are the shape and scale parameters of the Weibull distribution, respectively. The shape parameter (or Weibull modulus) is a dimensionless measure of the dispersion of strength while the scale parameter is the characteristic strength (at $P_f = 0.6321$) of a unit area of material in uniaxial tension. Note that dimensional compatibility means that σ_o has units of stress·area$^{1/m}$. An analogous equation based on component volume, V, can be shown for flaws that reside within the component.

Estimation of the Weibull parameters comes from rupture experiments of specimens (ideally 30 or more) in simple tension or flexure. Regression techniques such as least squares and maximum likelihood have been developed that can determine these parameters from a simplified form of equation (1);

$$\begin{aligned} P_f &= 1 - \exp\left[-\int_A \left(\frac{\sigma\ (x,y)}{\sigma_f} \right)^m\ dA\ \left(\frac{\sigma_f}{\sigma_o} \right)^m \right] \\ &= 1 - \exp\left[-A_e \left(\frac{\sigma_f}{\sigma_o} \right)^m \right] = 1 - \exp\left[-\left(\frac{\sigma_f}{\sigma_\theta} \right)^m \right] \end{aligned} \tag{2}$$

where σ_f is the peak stress in the specimen, σ_θ is the specimen characteristic strength, and A_e is known as the effective area. The characteristic strength, σ_θ , is the value of σ_f where $P_f = 0.6321$. A_e is an equivalent area that is a function of stress magnitude and Weibull modulus and not the true area of the component; it is calculated in the CARES/*Life* program. It can be thought of as the area of a baseline specimen subjected to a uniform stress that is equal to the peak stress in the component. Note that the strength anisotropy of the single crystal material was not accounted for here. The Principle of Independent Action model (described in ref. 17) was used for multiaxial stresses however for the specimens used here the first principal stress dominates the reliability response.

The Weibull size effect is a direct consequence of equation (1) and predicts that the average strength of a large component is lower than that for a smaller component for identical loading and geometry due to the increased probability of having a weaker flaw present. The magnitude of the size effect is a function of the effective area (or volume) and the Weibull modulus. For two different component geometry/loading combinations, the size effect strength ratio is obtained by equating the probabilities of failure for the two different components resulting in

$$\left(\frac{\sigma_{f,2}}{\sigma_{f,1}}\right)=\left(\frac{A_{e,1}}{A_{e,2}}\right)^{\frac{1}{m}}. \tag{3}$$

One can make a straightforward comparison between two components by determining the characteristic strength values $\sigma_{\theta,1}$ and $\sigma_{\theta,2}$ from the distributed strengths $\sigma_{f,1}$ and $\sigma_{f,2}$—that is the measure used here to test the applicability of the Weibull distribution to model the strength response of these materials at this size scale. The approach taken is that the Weibull parameters of the curve specimens are used as the baseline parameters which are assumed to describe the material. From that set of parameters the effective side-wall areas of the circle and ellipse specimens are computed from CARES/*Life* and results from finite element analysis using the average specimen dimensions. Predicted values of the characteristic strength for the circle and ellipse specimen geometries can then be obtained from equation (2). These predicted values of characteristic strength can be directly compared to measured values of characteristic strength obtained from the specimen rupture data.

Tables 4 and 5 present the measured σ_θ values for all three specimen and the predictions for the hole and ellipse specimens (based on the curve specimens) in tables 6 and 7. The complete set of Weibull parameters for the experimental results for Batch 6 and Batch 7 are also listed in tables 4 and 5. One outlier data point was removed from the Batch 6 room temperature ellipse set; otherwise all fracture data was included (without censoring) in the analysis. The scale parameter σ_o was calculated from CARES/*Life* based on the side-wall area of the specimens consistent with the approach taken in reference 22—that is, the scale parameter was calculated based on the Weibull modulus and characteristic strength that was measured for the respective specimen type. The maximum likelihood method (ref. 23) was used to compute the Weibull parameters in these tables and 90% confidence bounds on those parameters are also shown. The span of the confidence bound is sensitive to the number of specimens, *n*, tested. The Kolmogorov-Smirnov (K-S) and Anderson-Darling (A-D) goodness-of-fit significance levels are also provided in reference 17. These tests provide a significance level (given as a percentage) of how well the data fit the Weibull distribution. The A-D test is more sensitive to the tails of the distribution. Tables 6 and 7 show the Weibull parameters (based on the curve specimens) used for the CARES/*Life* analysis and the predicted results for σ_θ. The effective area A_e is for the side-walls and was determined using CARES/*Life*, results from finite element analysis, and the Weibull modulus for the curve specimens.

TABLE 4.—MEASURED WEIBULL PARAMETERS FOR BATCH 6

Temperature	Shape	*n*	*m*	*m*, 90 % confidence bound	σ_θ, GPa	σ_θ, 90% confidence bound, GPa	Side-wall σ_o, GPa.mm$^{2/m}$	K-S, %	A-D, %
24 °C	Curved	19	5.94	7.54 / 4.05	0.713	0.768 / 0.663	0.520	61	84
	Circle	19	3.68	4.67 / 2.51	1.368	1.543 / 1.216	0.394	59	31
	Ellipse	18	1.97	2.53 / 1.30	1.587	2.017 / 1.255	------	51	29
	Ellipse*	16	3.66	4.73 / 2.39	1.364	1.558 / 1.196	0.147	99	97
1000 °C	Curved	8	3.88	5.32 / 2.05	0.727	0.875 / 0.609	0.469	96	76
	Circle	10	4.42	5.99 / 2.45	1.302	1.514 / 1.126	0.433	68	47
	Ellipse	7	5.44	7.56 / 2.70	1.027	1.186 / 0.895	0.278	99	91

*With outlier removed

TABLE 5.—MEASURED WEIBULL PARAMETERS FOR BATCH 7

Temperature	Shape	*n*	*m*	*m*, 90 % confidence bound	σ_θ, GPa	σ_θ, 90% confidence bound, GPa	Side-wall σ_o, GPa.mm$^{2/m}$	K-S, %	A-D, %
24 °C	Curved	12	2.44	3.24 / 1.45	0.509	0.648 / 0.403	0.277	99	87
	Circle	9	5.44	7.47 / 2.87	1.338	1.527 / 1.179	0.526	99	92
	Ellipse	14	3.62	4.74 / 2.27	1.641	1.900 / 1.421	0.291	66	91
1000 °C	Curved	12	2.45	3.26 / 1.46	0.508	0.645 / 0.402	0.273	92	76
	Circle	9	5.60	7.68 / 2.95	1.139	1.295 / 1.007	0.458	99	98
	Ellipse	13	3.70	4.87 / 2.26	1.166	1.355 / 1.006	0.206	99	89

TABLE 6.—WEIBULL PARAMETERS USED FOR *CARES/Life* ANALYSIS AND PREDICTED RESULTS FOR BATCH 6

Temperature	Shape	*m*	Side-wall σ_o, GPa.mm$^{2/m}$	Side-wall A_e, mm^2	Predicted σ_θ, GPa
24 °C	Curved	5.94	0.520	0.153	------
	Circle			0.00549	1.249
	Ellipse			0.000639	1.794
1000 °C	Curved	3.88	0.469	0.183	------
	Circle			0.00941	1.561
	Ellipse			0.00132	2.591

TABLE 7.—WEIBULL PARAMETERS USED FOR CARES/*Life* ANALYSIS AND PREDICTED RESULTS FOR BATCH 7

Temperature.	Type	*m*	Side-wall σ_o, GPa.mm$^{2/m}$	Side-wall A_e, mm^2	Predicted σ_θ, GPa
24 °C	Curved	2.44	0.277	0.227	------
	Circle			0.0241	1.275
	Ellipse			0.00570	2.302
1000 °C	Curved	2.45	0.273	0.218	------
	Circle			0.0240	1.252
	Ellipse			0.00523	2.331

As can be seen from the tables, similar fracture strength patterns continued in Batch 7 as for Batch 6. That is, the strength remained independent of temperature for both the curve and circle specimens, while for the ellipse specimen the strength decreased at the elevated temperature. The curve strength decreased in Batch 7 (0.45 GPa) compared to Batch 6 (0.66 GPa), while both batches displayed the same strength for the other two specimen shapes. The Weibull modulus remained constant as a function of temperature for each specimen shape of Batch 7.

Figure 15 plots the results from tables 4 to 7 on a log-log plot. The abscissa is the ratio of A_e of the curve specimens to A_e of either the hole or ellipse specimens—the increasing numbers denote smaller highly stressed areas. The ordinate is the characteristic strength, σ_θ, and the experimental results are plotted with error bars that are the 90% confidence bounds. The CARES/*Life* predictions, extrapolated from the curve specimen results, are shown as lines which have slope 1/m.

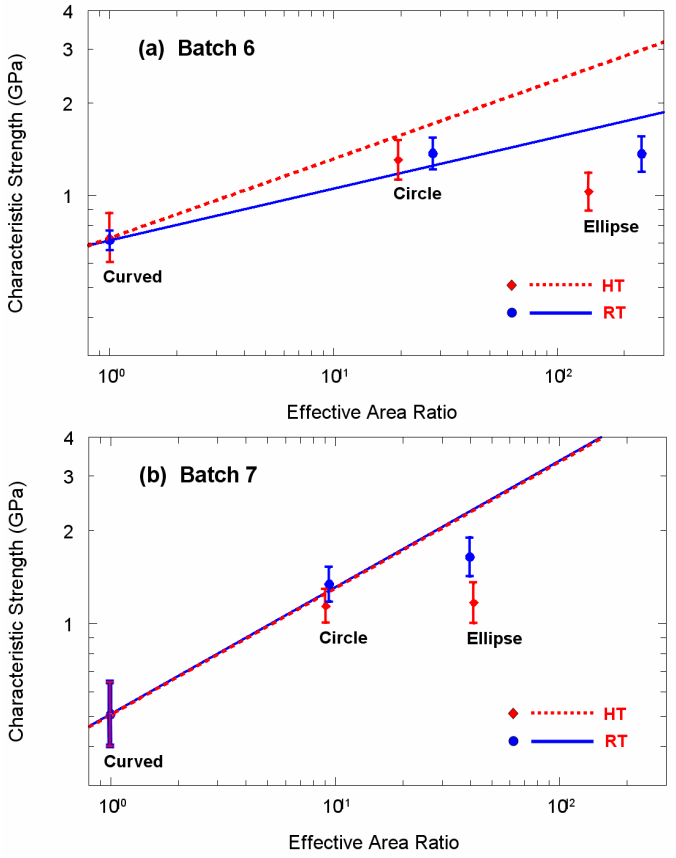

Figure 15.—(a) Batch 6, (b) Batch 7. room temperature (RT) (24 °C) and high temperature (HT) (1000 °C) characteristic strengths σ_θ versus side-wall effective area ratio (curve/hole or curve/ellipse). Error bars are 90% confidence bounds on the experimental characteristic strengths, and the lines represent predicted values from the curved specimens.

Figure 15 shows that the size effect for the circle specimens is predicted reasonably well by the Weibull distribution; however the same cannot be said for the ellipse specimens. The figures show that the strength of the curved specimens was not affected by temperature. For the circle specimens the strength at high temperature was somewhat lower but this was not necessarily significant since the confidence bounds overlapped. For the ellipse specimens strength degradation at high temperature appeared to be statistically significant. The strength degradation of the ellipse specimens at high temperature was an unexpected result.

The Batch 6 data for the circle specimens is bracketed by the room temperature and high temperature Weibull lines. Assuming that the curved specimens were not appreciably affected by temperature, then a Weibull modulus in-between the value for the RT and HT values would correlate very well to the data. For Batch 7, the predicted size effect and the observed size effect correlated very well at both temperature levels (and were nearly coincident) for the circle specimens. The ellipse specimens did not correlate well with the predictions in either case, particularly at high temperature. For the most part the ellipse specimens showed approximately the same strength response as the circle specimens.

The fact that two different material batches at two different temperatures—for a total of four experimental data sets—correlated well for the circle specimens is compelling evidence that the Weibull distribution could successfully predict strength response at least for moderate levels of stress concentration. However, there was an apparent lack of success in predicting the strengths for the ellipse specimens. A probabilistic simulation was demonstrated in reference 3 to account for the effect of the

scatter in specimen dimensions on the predicted strengths for the ellipse specimens for Batch 6 data at room temperature. That work showed that dimensional scatter did play a role in the predicted strengths of the ellipse specimens, but it also showed that the strengths of the ellipse specimens were still over-predicted.

Normally a change of strength with temperature is indicative of a change in stress intensity factor K_{Ic} or the presence of subcritical crack growth, but this behavior was not consistent across all the specimen types. One possible contributor to the lower than expected strengths would be increased surface roughness along the sidewalls of the ellipse, although this would not account for the additional high temperature degradation. It is known that differences in surface roughness do affect strength as shown in reference 24. Also, the ellipse specimens tested the limit of manufacturability with the current fabrication process. The modeled shape of the elliptical hole and the actual shape may have differed enough to cause some discrepancy.

For the sake of completeness the CARES/*Life* predictions of probability of failure versus strength are shown with the ranked fracture strengths, σ_f, of the individual specimens in figures 16 through 19. The failure probability for individual specimens is obtained from the median rank formula

$$P_{f,i} = \left(\frac{i - 0.5}{n} \right) \tag{4}$$

where $P_{f,i}$ is the failure probability of the i^{th} ranked (from lowest to highest) specimen and n is the total number of specimens in the set. Note that deviation of the data from the shape of the predicted curves is less significant when the number of specimens is small. This is born out by the fact that confidence bounds on Weibull parameters, particularly on m, are larger as the number of tested specimens, n, becomes smaller. Tables 4 and 5 show that there can be wide variation on m that is observed (estimated from the data) and hence correlation of the data to the shape of the predicted curve is not as important as correlation to the characteristic strength σ_θ.

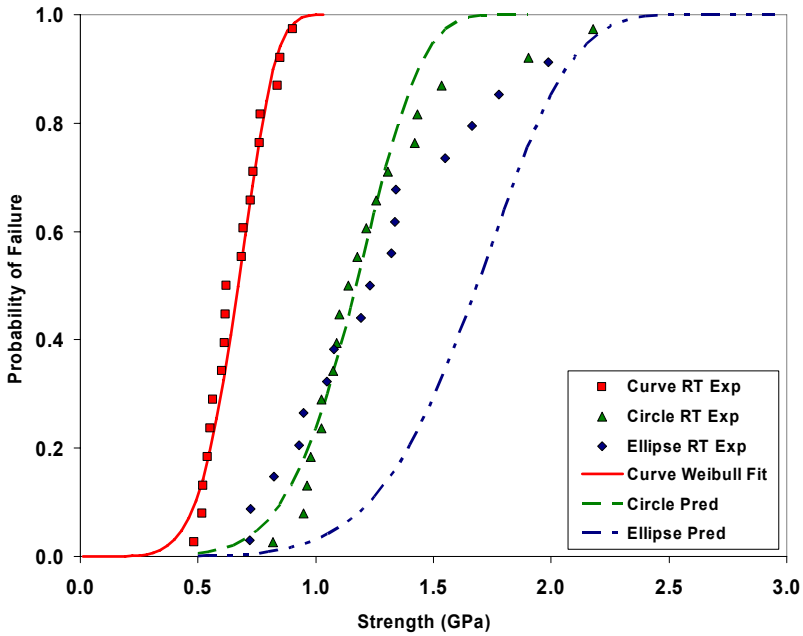

Figure 16.—Measured and predicted strengths for Batch 6 at RT.

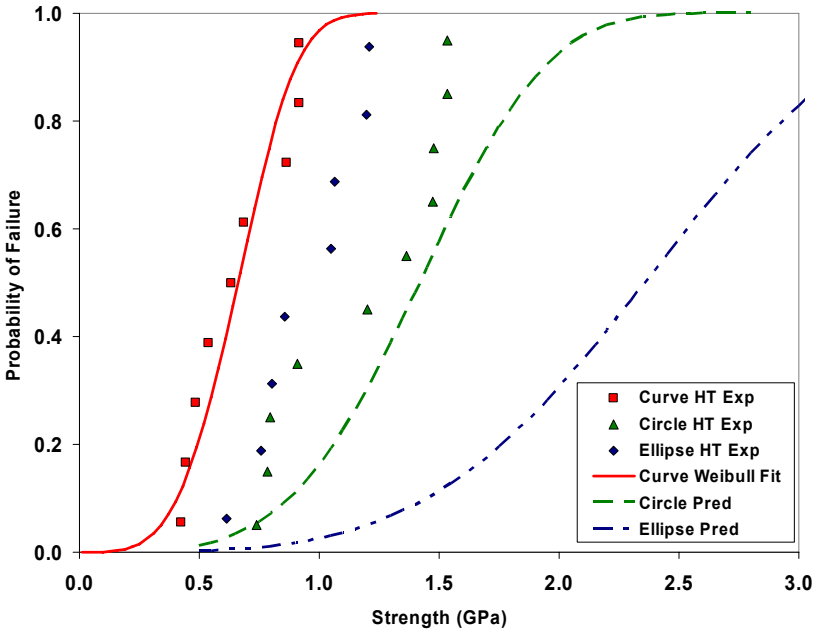

Figure 17.—Measured and predicted strengths for Batch 6 at 1000 °C.

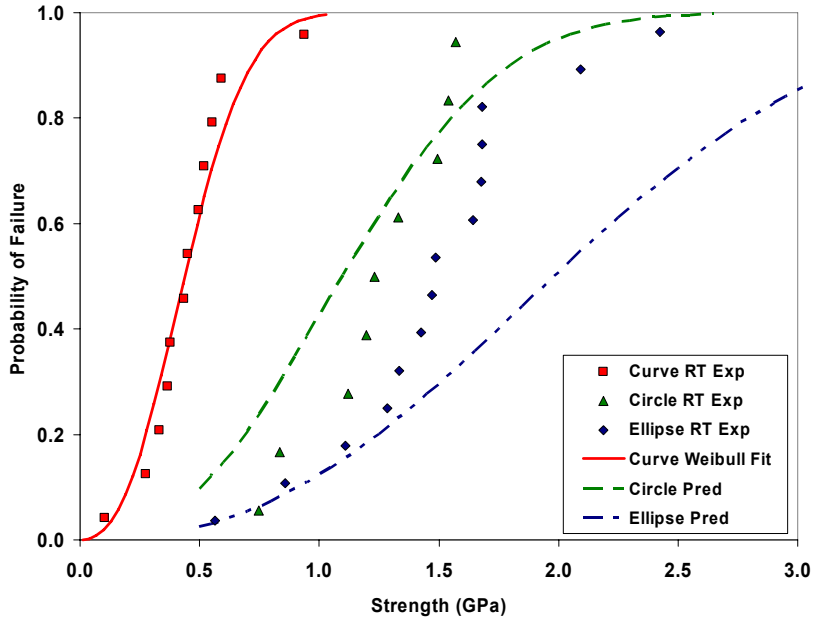

Figure 18.—Measured and predicted strengths for Batch 7 at RT.

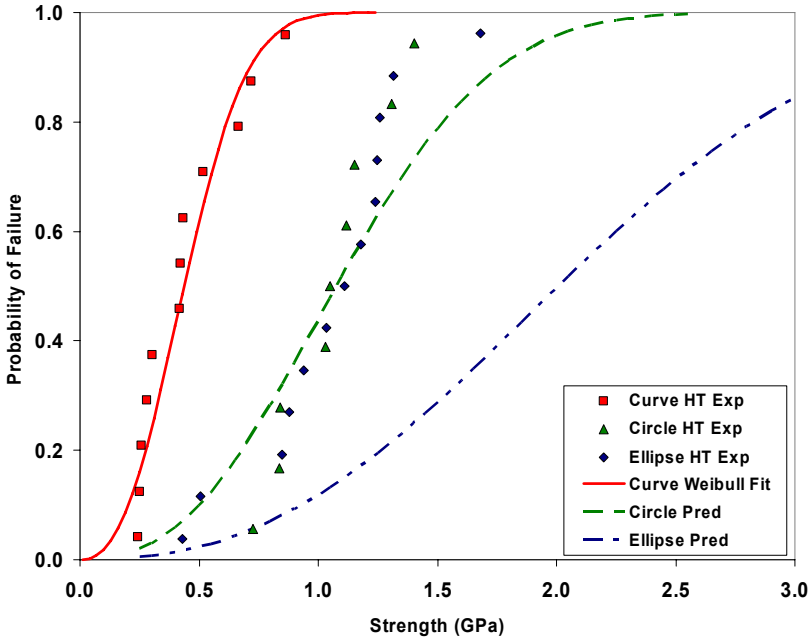

Figure 19.—Measured and predicted strengths for Batch 7 at 1000 °C.

Concluding Remarks

The specimen design and gripping system worked well. It is difficult to grip a brittle tensile specimen without generating fractures outside the gage section, but the wide wedge-shaped ends and the matching insert that gripped the insert along the sides of the wedge and the gentle curvature of the smooth specimens caused them to break near their centers. The stress concentrations of the circular and elliptical holes of course assure that the specimens break at the desired location.

It is not easy to test such small specimens at high temperatures. They can be heated resistively as has been done for titanium aluminide (ref. 25); this has the advantage that the grips, which must be electrically insulated, stay cool as do the load cell and actuator. While the temperature variation across the middle of a smooth specimen is acceptable, holes in a specimen would create large gradients that could affect the local fracture strength. A furnace with a uniform temperature distribution is therefore necessary, but this means that the grips must withstand the temperature as must a link to the outside load cell and actuator. A vertical orientation solves the problem of friction in the load train, but a key here was the ceramic grips that could be machined and then cured to the required tolerances.

The fracture strengths measured here were slightly smaller than obtained in thin-film polycrystalline silicon carbide specimens having a different shape and fabricated by different processes. They were similar in strength to an earlier series of polycrystalline silicon carbide specimens from NASA tested at room temperature. The fracture strengths of smooth silicon carbide specimens of all types tend to be in the 0.5 to 1.5 GPa range with coefficients of variation on the order of 30% in most cases. As one would expect, there is a lot of variation from batch to batch since the fracture strength is so dependent upon surface flaws.

Introducing stress concentrations and the finite element based CARES/*Life* analysis is a good way to study the effect of size on the fracture strength, but the difficulty in making uniform circular and elliptical holes adds to the scatter in the results. There is no change in fracture strength with temperature for the smooth specimens, but there is some decrease for the ones with holes. Whether this is caused by the non-uniformity of them is unclear. The analysis results showed that good to very good correlation was consistently obtained for the circle specimens while the correlation for the ellipse specimens was not good. This does not necessarily mean that the Weibull distribution could not predict the ellipse specimen

strength response; rather, it may indicate that the analysis did not account for all factors that significantly affected strength. Regardless, it seems safe to conclude that Weibull analysis was appropriate for at least moderate levels of stress concentration.

The strength results and the CARES/*Life* analysis show that local tensile stress levels would have to be kept very low for silicon carbide to function as a structural material in MEMS. However, the fact that the material maintains its strength at elevated temperatures (at least at moderate stress concentrations) makes it attractive for applications in that environment.

References

1. S.M. Spearing, "Materials Issues in Microelectromechanical Systems (MEMS)" *Acta Materialia*, vol. 48, pp. 179-196, 2000.
2. W.N. Sharpe, Jr., O. Jadaan, G.M. Beheim, G.D. Quinn, and N.N. Nemeth, "Fracture Strength of Silicon Carbide Microspecimens," *Journal of Microelectromechanical Systems*, vol. 14, pp. 903-13, 2005.
3. N.N. Nemeth, L.J. Evans, O.M. Jadaan, W.N. Sharpe, and G.M. Beheim, "Fabrication and Probabilistic Fracture Strength Prediction of High-Aspect-Ratio Single Crystal Silicon Carbide Microspecimens with Stress Concentration," *Thin Solid Films*, vol. 515, pp. 3283-3290, 2007.
4. W.N. Sharpe, Jr., G.M. Beheim, N.N. Nemeth, L. Evans, and O. Jadaan, "Strength of Single-Crystal Silicon Carbide Microspecimens at Room and High Temperature," *Proceedings of the 2005 SEM Annual Conference and Exposition on Experimental and Applied Mechanics*, pp. 1095-1101, 2005.
5. Harris, G.L., "Properties of Silicon Carbide," Institution of Engineering and Technology, 1995.
6. Mehregany, M., Zorman, C.A., Rajan, N., and Chien Hung Wu, "Silicon Carbide MEMS for Harsh Environments," *Proceedings of the IEEE*, vol. 86, pp. 1594-1609, 1998.
7. J.M. Melzak, "Silicon Carbide for RF MEMS," *IEEE MTT-S International Microwave Symposium Digest*, vol. 3, pp. 1629-1632, 2003.
8. H-S. Moon, D. Choi, and S.M. Spearing, "Development of Si-SiC Hybrid Structures for Elevated Temperature Micro-Turbomachinery," *Journal of Microelectromechanical Systems*, vol. 13, pp. 676-687, 2004.
9. Shackelford, J.F., Editor, "CRC Materials Science and Engineering Handbook," CRC Press, Boca Raton, FL, 2001.
10. J.S. Mitchell, C.A. Zorman, T. Kicher, S. Roy, and M. Merhregany, "Examination of Bulge Test for Determining Residual Stress, Young's Modulus, and Poisson's Ratio of 3C-SiC Thin Films," *Journal of Aerospace Engineering*, vol. 16, pp. 46-54, 2003.
11. C. Serre, A. Perez-Rodriguez, A. Romano-Rodriguez, J.R. Morante, J. Esteve, and A. Cruz, "Test Microstructures for Measurement of SiC Thin Film Mechanical Properties," *Journal of Micromechanics and Microengineering*, vol. 9, pp. 190-193,1999.
12. C.M. Su, M. Wuttig, A. Fekade, and M. Spencer, "Elastic and Anelastic Properties of Chemical Vapor Deposited Epitaxial 3C-SiC," *Journal of Applied Physics*, vol. 77, pp. 5611-5615, 1995.
13. K.M. Jackson, J. Dunning, C.A. Zorman, M. Mehregany, and W. N. Sharpe, Jr. "Mechanical Properties of Epitaxial 3C Silicon Carbide Thin Films," *Journal of Microelectromechanical Systems*, vol.14, pp. 664-672, 2005.
14. K.M. Jackson, "Fracture Strength, Elastic Modulus and Poisson's Ratio of Polycrystalline 3C Thin-Film Silicon Carbide Found by Microsample Tensile Testing," *Sensors and Actuators A (Physical)*, vol.125, pp. 34-40, 2005.
15. S.R. Choi, L.M. Powers, and N.N. Nemeth, "Slow Crack Growth Behavior and Life/Reliability Analysis of 96 wt% Alumina at Ambient Temperature With Various Specimen/Loading Configurations," NASA/TM—2000-210206, July 2000.
16. N.N. Nemeth, L.M. Powers, L.A. Janosik, and J.P. Gyekenyesi, "Designing Ceramic Components for Durability," *American Ceramics Society Bulletin*, vol. 72, pp. 59-69, 1993.

17. N.N. Nemeth, L.M. Powers, L.A. Janosik, and J.P. Gyekenyesi, "Ceramics Analysis and Reliability Evaluation of Structures Life Prediction Program Users and Programmers Manual," *NASA/TM-2003-106316*, 2003.
18. W.N. Sharpe, Jr., D. Danley, and D. LaVan, "Microspecimen Tensile Tests of A533-B Steel," *Small Specimen Test Techniques, ASTM STP 1329, American Society for Testing And Materials*, pp. 497-512, 1998.
19. Cree Materials, 2005, "Silicon Carbide Substrates," *MAT-CATALOG.00D, Cree Materials, 4600 Silicon Drive, Durham, NC, 27703,* WWW.cree.com/ftp/pub/sicctlg_read_new.pdf
20. L.J. Evans and G.M. Beheim, "Deep Reactive Ion Etching (DRIE) of High Aspect Ratio SiC Microstructures using a Time-Multiplexed Etch-Passivate Process," Materials Science Forum Vols. 527-529, pp 1115-8, 2006.
21. F. Laermer and A. Urban, "Challenges, Developments and Applications of Silicon Deep Reactive Ion Etching," *Microelectronics Engineering*, vol. 67-68, pp. 349-355, 2003.
22. Bagdahn, J., Sharpe, W.N., Jr., and Jadaan O. , "Fracture Strength of Polysilicon at Stress Concentrations," *Journal of Microelectromechanical Systems*, vol. 12, pp. 302-312, 2003.
23. Thoman, D.R., Bain, L.J., and Antle, C.E., "Inferences on the Parameters of the Weibull Distribution," *Technomet*, vol. 11, pp. 445–460, 1969.
24. Chen, K., Ayon, A., and Spearing, S.M., "Controlling and Testing the Fracture Strength of Silicon on the Mesoscale." *Journal of the American Ceramic Sociey*, vol. 83, pp. 1476-1480, 2000.
25. M. Zupan, M. J. Hayden, C.J. Boehlert, and K.J. Hemker, "Development of High-Temperature Microsample Testing," *Experimental Mechanics*, vol. 41, pp. 242-247, 2001.

REPORT DOCUMENTATION PAGE	Form Approved OMB No. 0704-0188

1. REPORT DATE *(DD-MM-YYYY)*	2. REPORT TYPE	3. DATES COVERED *(From - To)*
01-10-2007	Technical Memorandum	

4. TITLE AND SUBTITLE
Fracture Strength of Single-Crystal Silicon Carbide Microspecimens at Room and Elevated Temperature

5a. CONTRACT NUMBER

5b. GRANT NUMBER

5c. PROGRAM ELEMENT NUMBER

6. AUTHOR(S)
Nemeth, Noel, N.; Sharpe, William, N., Jr.; Beheim, Glenn, M.; Evans, Laura, J.; Jadaan, Osama, M.

5d. PROJECT NUMBER

5e. TASK NUMBER

5f. WORK UNIT NUMBER
WBS 984754.02.07.03.19.05

7. PERFORMING ORGANIZATION NAME(S) AND ADDRESS(ES)
National Aeronautics and Space Administration
John H. Glenn Research Center at Lewis Field
Cleveland, Ohio 44135-3191

8. PERFORMING ORGANIZATION REPORT NUMBER
E-16167

9. SPONSORING/MONITORING AGENCY NAME(S) AND ADDRESS(ES)
National Aeronautics and Space Administration
Washington, DC 20546-0001

10. SPONSORING/MONITORS ACRONYM(S)
NASA

11. SPONSORING/MONITORING REPORT NUMBER
NASA/TM-2007-214990

12. DISTRIBUTION/AVAILABILITY STATEMENT
Unclassified-Unlimited
Subject Category: 37
Available electronically at http://gltrs.grc.nasa.gov
This publication is available from the NASA Center for AeroSpace Information, 301-621-0390

13. SUPPLEMENTARY NOTES

14. ABSTRACT
Three shapes of tensile specimens were tested--curved with a very low stress concentration factor and straight with either a circular hole or an elliptical hole. The nominal thickness was 125 μm with a net section 100 μm wide; the overall length of these microspecimens was 3.1 mm. They were fabricated by an improved version of deep reactive ion etching, which produced specimens with smooth sidewalls and cross-sections having a slightly trapezoidal shape that was exaggerated inside the holes. The novel test setup used a vertical load train extending into a resistance furnace. The specimens had wedge-shaped ends which fit into ceramic grips. The fixed grip was mounted on a ceramic post, and the movable grip was connected to a load cell and actuator outside the furnace with a ceramic-encased nichrome wire. The same arrangement was used for tests at 24 and at 1000 °C. The strengths of the curved specimens for two batches of material (made with slightly different processes) were 0.66 ± 0.12 GPa and 0.45 ± 0.20 GPa respectively at 24 °C with identical values at 1000 °C. The fracture strengths of the circular-hole and elliptical-hole specimens (computed from the stress concentration factors and measured loads at failure) were approximately 1.2 GPa with slight decreases at the higher temperature. Fractographic examinations showed failures initiating on the surface--primarily at corners. Weibull predictions of fracture strengths for the hole specimens based on the properties of the curved specimens were reasonably effective for the circular holes, but not for the elliptical holes.

15. SUBJECT TERMS
Reliability analysis; Ceramics; Weibull density function; MEMS; Silicone carbide

16. SECURITY CLASSIFICATION OF:			17. LIMITATION OF ABSTRACT	18. NUMBER OF PAGES	19a. NAME OF RESPONSIBLE PERSON
a. REPORT	b. ABSTRACT	c. THIS PAGE			STI Help Desk (email:help@sti.nasa.gov)
U	U	U	UU	26	19b. TELEPHONE NUMBER *(include area code)* 301-621-0390